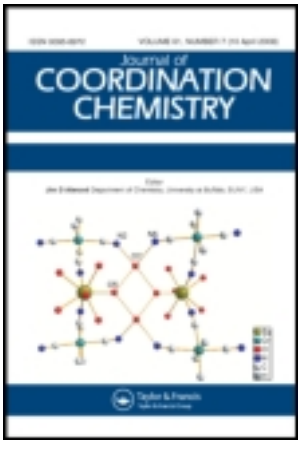

Journal of Coordination Chemistry
Publication details, including instructions for authors and subscription information:
http://www.tandfonline.com/loi/gcoo20

Studies on DNA binding, electrochemical activation, DNA photocleavage, and biopotency of N and O donor bidentate ligands with Cu(II), Co(II), and Zn(II)

N. Raman [a] & A. Selvan [a]
[a] Research Department of Chemistry , VHNSN College, Madurai Kamaraj University , Virudhunagar 626 001, India
Published online: 24 Jan 2011.

To cite this article: N. Raman & A. Selvan (2011) Studies on DNA binding, electrochemical activation, DNA photocleavage, and biopotency of N and O donor bidentate ligands with Cu(II), Co(II), and Zn(II), Journal of Coordination Chemistry, 64:3, 534-553, DOI: 10.1080/00958972.2010.551767

To link to this article: http://dx.doi.org/10.1080/00958972.2010.551767

Journal of Coordination Chemistry
Vol. 64, No. 3, 10 February 2011, 534–553

Studies on DNA binding, electrochemical activation, DNA photocleavage, and biopotency of N and O donor bidentate ligands with Cu(II), Co(II), and Zn(II)

N. RAMAN* and A. SELVAN

Research Department of Chemistry, VHNSN College, Madurai Kamaraj University, Virudhunagar 626 001, India

(*Received 15 September 2010; in final form 16 November 2010*)

Three Schiff-base ligands, namely 2-(3,4-dimethoxybenzylideneamino)phenol (**HL**^{1}), 2-(3-hydroxy-4-nitrobenzylidene-amino)phenol (**HL**^{2}), and 2-(3-methoxy-4-hydroxy-benzylideneamino)phenol (**HL**^{3}) and their Cu(II), Co(II), and Zn(II) complexes were synthesized and characterized by spectroanalytical techniques. The UV-Vis and magnetic moment data revealed square-planar Cu(II) and tetrahedral Co(II) and Zn(II). Conductivity data showed the non-electrolytic nature of the complexes. Absorption and viscometric titration as well as cyclic voltammetry studies revealed the complexes as avid binders of calf thymus (CT) DNA through intercalation. A profound effect of substituents on the Schiff base was observed on binding of complexes to CT-DNA and in cleavage of supercoiled pBR322 DNA. All the complexes showed DNA cleavage in the presence of mercaptopropionic acid (MPA) except **HL**^{1} complexes. The cleavage activity increased with longer exposure time of irradiation at 365 nm and higher complex concentration. The cleavage reactions in the presence of MPA involve hydroxyl radical. The synthesized Schiff bases and their metal complexes were also tested for antibacterial and antifungal activities. The metal complexes exhibited higher antibacterial and antifungal activities than the parent ligands and their biopotency is discussed.

Keywords: Electrochemistry; DNA interaction; DNA photocleavage; Antimicrobial

1. Introduction

Bidentate Schiff bases and their metal complexes have significant importance in biological processes and constitute an active area of research in modern coordination chemistry. The high affinity of Schiff bases for chelation to transition metal ions is utilized in preparing complexes. Compared with research on tridentate, quadridentate, macrocyclic, and acyclic hydroxy Schiff bases [1], very little attention has been focused on complexes of bidentate hydroxy Schiff bases [2]. Chelating ligands containing nitrogen and oxygen donors show broad biological activities and are of special interest because of their coordination to metals at active sites of metallobiomolecules [3]. Copper participates in transmutation and collagenation whereas other metals

*Corresponding author. Email: drn_ raman@yahoo.co.in

Journal of Coordination Chemistry
ISSN 0095-8972 print/ISSN 1029-0389 online © 2011 Taylor & Francis
DOI: 10.1080/00958972.2010.551767

participate in natural biological systems [4]. Metal ions bonded to biologically active compounds may enhance their antibacterial, antifungal, and anticancer activities [5].

Design of molecules capable of targeting specific DNA sites offers possibilities in developing tools for both pharmaceuticals and biotechnology [6]. Metal complex can bind to DNA non-covalently, with electrostatic effect, groove binding, and intercalation. Applications of metal complexes require that complexes bind to DNA through intercalation inducing cellular degradation [7]. The intercalating ability not only correlates with the planarity of ligand [8], but also relates to coordination geometry of the metal ion and donor type of the ligand [9]. Metal ion type and valency also play important roles in deciding the binding extent of complexes to DNA [10]. Copper complexes are widely used as DNA foot printing, DNA structural probes, potential anticancer drugs, etc. Changes in intensities of electronic spectra can be used to explain the nature and strength of stacking interactions between chromophores and DNA base pairs. There has been considerable interest in DNA photocleavage reactions activated by metal ions [11].

Herein, we investigate the ligation of Schiff bases derived from 2-aminophenol and disubstituted benzaldehydes and their complexes of Cu(II), Co(II), and Zn(II). Based on the literature [12, 13], we have synthesized disubstituted $\mathbf{HL^1}$ and $\mathbf{HL^3}$ and designed and synthesized the Schiff base $\mathbf{HL^2}$ to discuss the effect of substituents on biological studies. This article focuses on exploring the DNA-binding affinities of the metal complexes using electronic absorption, cyclic voltammetry (CV), and viscosity measurements. Ability to induce cleavage of pBR322 DNA and understand recognition of DNA by small ligands or metal complexes is crucial for development of drugs targeted at DNA. Our results on further understanding of DNA binding, efficiency of DNA recognition, and cleavage by metal(II) complexes lay the foundation for design of new photoprobes and photonucleases of DNA.

2. Experimental

2.1. *General measurements and materials*

All reagents were purchased from the commercial sources as reagent grade. Calf thymus (CT) DNA was obtained from the Sigma Company. All solvents were purified by regular methods. *Tris*-HCl buffer (5 mmol L^{-1} *Tris*-HCl, 50 mmol L^{-1} NaCl, pH, 7.2, *Tris* = *Tris*(hydroxymethyl)aminomethane) solution was prepared using deionized double-distilled water. UV-Vis spectra were recorded on a Shimadzu Model 1601 UV-Visible Spectrophotometer. CV measurements were performed at room temperature on a CHI 620C electrochemical analyzer in freshly distilled DMF. The X-band EPR spectra of the complexes were recorded on a Jeol RE2X electron spin resonance spectrometer at RT (300 K) and LNT (77 K) using TCNE as the g-marker. Thermogravimetric analysis (TGA) was carried out in dynamic air at a heating rate of 10°C min^{-1} using a Mettler Toledo System. X-ray diffraction (XRD) experiments were carried out on XPERT-PRO diffractometer system. Cu-Kα_1 line, with a wavelength of 1.5406 Å generated with a setting of 30 mA and 40 kV with the electrodes, was used for diffraction. The slit width setting was 91 mm. The diffracting angle (2θ) was scanned from 10.0251 to 79.9251 continuously with a rate of 2° per

minute at 25°C. Scanning Electron Micrography performed on SEM, JEOL JSM Model 6360, was used for morphological eva1uation. FTIR spectra were obtained on a Perkin-Elmer Paragon 1000 FTIR spectrophotometer equipped with KBr pellets using the diffuse reflectance technique (4000–400 cm^{-1}). Microanalyses were performed on a Perkin-Elmer 240 elemental analyzer. ^{1}H-NMR spectra were recorded on a Bruker (300 MHz) spectrometer. Mass spectrometry experiments were performed on a JEOL-AccuTOF JMS-T100LC mass spectrometer equipped with a custom-made electrospray interface. Room temperature magnetic susceptibility measurements were carried out on a modified Gouy-type magnetic balance, Hertz SG8-5HJ. The molar conductivity was measured for (10^{-3} mol L^{-1}) DMF solutions using a conductometer model 601/602.

2.2. *DNA binding and cleavage experiments*

DNA binding and cleavage experiments were performed at room temperature. The absorption titrations of Cu(II) and Co(II) complexes in *Tris*-HCl buffer (5 mmol L^{-1} *Tris*-HCl, 50 mmol L^{-1} NaCl, pH, 7.2) were performed by a fixed complex concentration to which increments of the DNA stock solution were added. Complex solutions employed were 25 μmol L^{-1} in concentration and CT-DNA was added at a ratio of 2 : 1 [DNA] : [complex]. Complex-DNA solutions were allowed to incubate for 10 min before absorption spectra were recorded. The intrinsic binding constant ratio K_b of Cu(II) and Co(II) complexes to DNA was calculated using the following equation:

$$[DNA]/(\varepsilon_a - \varepsilon_f) = [DNA]/(\varepsilon_b - \varepsilon_f) + 1/[K_b(\varepsilon_b - \varepsilon_f)],$$

where [DNA] is the concentration of DNA in base pairs, ε_a, ε_f, and ε_b are the apparent, free, and bound metal complexes extinction coefficients, respectively. In plots of $[DNA]/(\varepsilon_a - \varepsilon_f)$ *versus* [DNA], K_b is given by the ratio of slope to the intercept.

CV was carried out at different scan rates in DMF to determine the binding affinity between DNA and complexes using a three-electrode configuration (glassy carbon working electrode, Pt counter electrode, and Ag/AgCl reference electrode). All the samples were purged with nitrogen prior to measurements.

Viscosity measurements were carried out using an Ubbelodhe viscometer maintained at a constant temperature of 25°C in a thermostated water bath. Flow time was measured with a digital stopwatch with each sample measured three times and an average flow time calculated. Data are presented as $(\eta/\eta^o)^{1/3}$ *versus* binding ratio, where η is the viscosity of CT-DNA in the presence of complex and η^o is the viscosity of CT-DNA alone.

For the gel electrophoresis experiments, supercoiled (SC) circular pBR322 DNA (0.5 μg) was treated with complexes in 50 mmol L^{-1} *Tris*-HCl buffer (pH 7.2) containing 50 mmol L^{-1} NaCl in the presence and absence of reducing agent in the dark, then irradiated at room temperature with a UV-light (365 nm) for 45 min.

Inhibition reactions for the "chemical nuclease" reactions were carried out in the dark in the presence of reagents like distamycin (100 μmol L^{-1}) and DMSO (4 μL) prior to addition of complexes and the reducing agent 3-mercaptopropionic acid (MPA). Inhibition reactions for the photo-induced DNA cleavage study were carried out at 365 nm using reagents, namely NaN_3 (5 μL), ethanol (4 μL), KI (4 μL), DMSO (4 μL), and histidine (50 μmol L^{-1}) prior to the addition of the complexes. For the D_2O experiment, this solvent was used for dilution of the sample to 10 μL. The samples after

incubation for 1 h at 37°C in a dark chamber were added to the loading buffer containing 25% bromophenol blue, 0.25% xylene cyanol, 30% glycerol (3 μL) and the samples were analyzed by electrophoresis for 30 min at 50 V in 50 mmol L^{-1} *Tris*-HCl buffer (pH 7.2) containing 0.8% agarose gel. The gel was stained with 1 μg (mol^{-1}) ethidium bromide (EB) and then photographed under UV light.

2.3. *Microbial assay*

The Schiff-base metal(II) complexes were tested for their effect on certain pathogenic bacteria and fungi by the disc diffusion method [14]. The complexes were stored dry at room temperature and dissolved in DMF (1%). Both Gram-positive (*Staphylococcus aureus*, *Bacillus subtilis*) and Gram-negative (*Escherichia coli*, *Pseudomonas aeruginosa*) bacteria were grown in nutrient agar medium and incubated at 37°C for 48 h followed by frequent subculture to fresh medium and were used as test bacteria. The *Aspergillus niger*, *Rhizopus stolonifer*, *Candida albicans*, and *Rhizoctonia bataticola*, used as test fungi, were grown into dextrose agar medium and incubated at 27°C for 72 h followed by periodic subculturing to fresh medium. Then the Petri discs were inoculated with a loop full of bacterial or fungal culture and spread throughout the Petri discs uniformly with a sterile glass spreader. To each disc, the test samples (10 μg mL^{-1}) and reference streptomycin (5 μg $disc^{-1}$ for bacteria) or nystatin (10 μg $disc^{-1}$ for fungi) were added with a sterile micropipette. The plates were then incubated at 35 ± 2°C and 27 ± 1°C for bacteria and fungi, respectively, and growth of microorganisms was observed. When no growth of microorganisms was observed in the medium containing the lowest concentration of test materials, the minimum inhibitory concentration (MIC) of the test material was defined at this point of dilution. The MIC was measured to be the lowest concentration after the period of incubation.

2.4. *Synthesis and characterization of ligands*

The Schiff-base ligands 2-(3,4-dimethoxybenzylideneamino)phenol (**HL^1**) and 2-(3-methoxy-4-hydroxy-benzylideneamino)phenol (**HL^3**) were synthesized according to literature procedures [12, 13] whereas another Schiff-base ligand 2-(3-hydroxy-4-nitrobenzylidene-amino)phenol (**HL^2**) was prepared by condensation of *o*-hydroxyaniline (1.09 g, 0.01 mol) with 3-hydroxy-4-nitrobenzaldehyde (1.67 g, 0.01 mol) refluxed in ethanol for 3 h, then cooled to room temperature to give a precipitate which was collected and then washed with ethanol.

HL^1: light brown powder, yield 75%, molecular formula: $C_{15}H_{15}NO_3$, molecular weight: 257.28, m.p.: 98°C, Anal. Calcd C(70.02%), H(5.87%), N(5.44%); found: C(69.85%), H(5.75%), N(5.42%); ^{1}H-NMR (300 MHz, DMSO-d_6) δ: 3.97(S, 3H, O–CH_3), 9.86(s, 1H, OH), 6.78–7.18(m, 4H, Ph), 7.26–7.58(m, 3H, Ph), 8.60(s, 1H, N=CH) IR(KBr) γ (cm^{-1}): 1620(s) (HC=N), 1374(m) (O–CH_3), 1328(m) (C–O), 2845(m) (O–H $\cdots$ N), 1416(s) (Ph–C=C), 1515(m) (Ph–C–C), 2936(s) (Ph–C–H) UV-Vis (DMF) [nm (frequency, cm^{-1}) (transition)]; 308(32,467) (intra ligand charge transfer) (ILCT), 275(36,363) (ILCT), 268(37,313) (ILCT), 254(39,370) (ILCT).

HL^2: yellow powder, yield 82%, molecular formula: $C_{13}H_{10}N_2O_4$, molecular weight: 258.13, m.p.: 182°C, Anal. Calcd C(60.46%), H(3.90%), N(10.84%); found: C(60.38%), H(3.91%), N(10.83%); ^{1}H-NMR (300 MHz, DMSO-d_6) δ: 10.57(s, 1H, OH), 6.73–7.02(m, 4H, Ph), 7.21–7.62(m, 3H, Ph), 8.55(s, 1H, N=CH) IR(KBr) γ (cm^{-1}): 1625(s) (HC=N), 1620(m) (C–NO_2), 3381(b) (free OH), 1321(m) (C–O), 2852(w) (O–H $\cdots$ N), 1431(m) (Ph–C=C), 1531(m) (Ph–C–C), 2925(m) (Ph–C–H) UV-Vis (DMF) [nm (frequency, cm^{-1})(transition)]; 350(28,571) (ILCT), 265(37,735) (ILCT), 248(40,323) (ILCT).

HL^3: brown powder, yield 78%, molecular formula: $C_{14}H_{13}NO_3$, molecular weight: 243.26, m.p.: 88°C, Anal. Calcd C(69.12%), H(5.38%), N(5.75%); found C(69.13%), H(5.33%), N(5.73%); ^{1}H-NMR (300 MHz, DMSO-d_6) δ: 3.96(s, 3H, O–CH_3), 10.13(s, 1H, OH), 6.75–7.12(m, 4H, Ph), 7.25–7.55(m, 3H, Ph), 8.48(s, 1H, N=CH), IR(KBr) γ (cm^{-1}): 1615(s) (HC=N), 1331(s) (O–CH_3), 3444(b) (free OH), 1332(m) (C–O), 2849(w) (O–H $\cdots$ N), 1416(m) (Ph–C=C), 1515(m) (Ph–C–C), 2940(s) (Ph–C–H) UV-Vis (DMF) [nm (frequency, cm^{-1})(transition)]; 361(27,701) (ILCT), 265(37,735) (ILCT), 251(39,840) (ILCT).

2.5. *Synthesis and characterization of metal complexes*

The synthetic route to the complexes is summarized in scheme 1. All the complexes were synthesized by mixing ethanolic solution of ligands and metal(II) salts in required molar ratio (1 : 2). The reaction mixture was refluxed on a water bath for 2–3 h and then concentrated to a small volume on a hot plate at ~50°C. After cooling, the solid complexes were filtered, recrystallized, washed in ethanol, and dried in vacuum over $CaCl_2$.

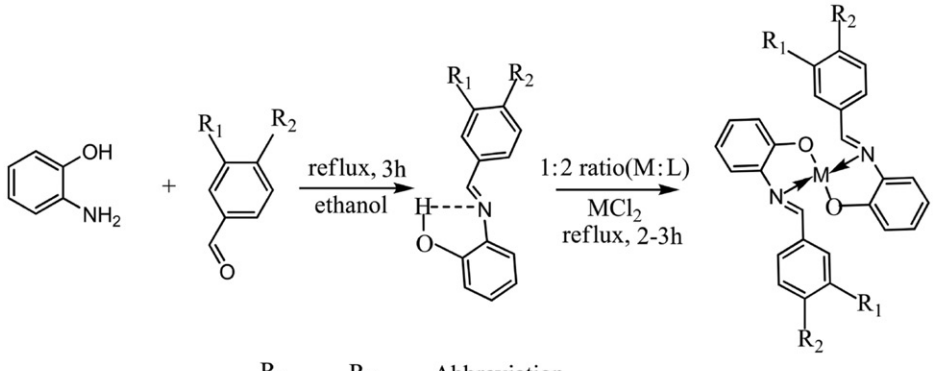

R_1	R_2	Abbreviation	
OCH_3	OCH_3	HL^1	**1a**
OH	NO_2	HL^2	**2b**
OCH_3	OH	HL^3	**3c**

Scheme 1. Synthetic route for preparation of the complexes, where M = Cu(II), Co(II), and Zn(II).

CuL_2[1a] (1): black, yield 65%, molecular formula: $CuC_{30}H_{28}N_2O_6$, molecular weight: 576.10, m.p.: 194°C, Anal. Calcd C(62.54%), H(4.89%), N(4.86%), Cu(11.03%); found: C(62.51%), H(4.91%), N(4.85%), Cu(11.01%); IR(KBr) ν (cm^{-1}): 1584(s) (HC=N), 1370(w) (O–CH_3), 1317(m) (C–O), 421(m) (M–N), 557(m) (M–O), 1421(s) (Ph–C=C), 1496(m) (Ph–C–C), 2963(s) (Ph–C–H) UV-Vis (DMF) [nm (frequency, cm^{-1})(transition)(geometry)]; 503(19,880) ($^2B_{1g} \rightarrow {}^2A_{1g}$)(square-planar; SP), 417 (23,980) ($^2B_{1g} \rightarrow {}^2E_{1g}$) (SP), 268(37,313) (ILCT) magnetic moment, μ_{eff} (BM); 1.68.

CuL_2[2b] (2): black, yield 73%, molecular formula: $CuC_{26}H_{18}N_4O_8$, molecular weight: 577.99, m.p.: 127°C, Anal. Calcd C(54.02%), H(3.14%), N(9.71%), Cu(10.99%); found: C(53.97%), H(3.12%), N(9.68%), Cu(10.96%); IR(KBr) ν (cm^{-1}): 1585(s) (HC=N), 1620(m) (C–NO_2), 3375(w) (free OH), 1312(m) (C–O), 417(m) (M–N), 538(s) (M–O), 1472(m) (Ph–C=C), 1534(m) (Ph–C–C), 2924(m) (Ph–C–H) UV-Vis (DMF) [nm (frequency, cm^{-1})(transition)(geometry)]; 508(19,685) ($^2B_{1g} \rightarrow {}^2A_{1g}$)(SP), 435(22,988) ($^2B_{1g} \rightarrow {}^2E_{1g}$) (SP), 350(28571) (ILCT), 265(37,735) (ILCT) magnetic moment, μ_{eff} (BM); 1.71.

CuL_2[3c] (3): brown, yield 68%, molecular formula: $CuC_{28}H_{24}N_2O_6$, molecular weight: 548.05, m.p.: >250°C, Anal. Calcd C(61.36%), H(4.41%), N(5.11%), Cu(11.59%); found: C(61.29%), H(4.37%), N(4.95%), Cu(10.98%); IR(KBr) ν (cm^{-1}): 1585(m) (HC=N), 1328(m) (O–CH_3), 3401–3443(b) (free OH), 1321(m) (C–O), 415(m) (M–N), 570(s) (M–O), 1414(m) (Ph–C=C), 1518(m) (Ph–C–C), 2933(w) (Ph–C–H) UV-Vis (DMF)[nm (frequency, cm^{-1})(transition)(geometry)]; 535(18,691) ($^2B_{1g} \rightarrow {}^2A_{1g}$)(SP), 416(24,038) ($^2B_{1g} \rightarrow {}^2E_{1g}$) (SP), 265(37,735) (ILCT), 229(43,668) (ILCT) magnetic moment, μ_{eff} (BM); 1.65.

CoL_2[1a] (4): light brown, yield 66%, molecular formula: $CoC_{30}H_{28}N_2O_6$, molecular weight: 571.49, m.p.: 188°C, Anal. Calcd C(63.05%), H(4.93%), N(4.90%), and Co(10.31%); found: C(62.96%), H(4.91%), N(4.83%), and Co(10.28%); IR(KBr) ν (cm^{-1}): 1587 (s) (HC=N), 1363(w) (O–CH_3), 1315(m) (C–O), 428(m) (M–N), 565(s) (M–O), 1428(m) (Ph–C=C), 1485(m) (Ph–C–C), 2972(s) (Ph–C–H) UV-Vis (DMF) [nm (frequency, cm^{-1})(transition)(geometry)]; 581(17,211) [$^4T_1(F) \rightarrow {}^4A_2(F)$] (tetrahedral), 435(22,988) [$^4T_1(F) \rightarrow {}^4T_1(P)$] (tetrahedral), 308(32,467) (ILCT), 275(36,363) (ILCT) magnetic moment, μ_{eff} (BM); 4.28.

CoL_2[2b] (5): brown, yield 78%, molecular formula: $CoC_{26}H_{18}N_4O_8$, molecular weight: 573.38, m.p.: 153°C, Anal. Calcd C(54.46%), H(3.16%), N(9.77%), Co(10.27%); found: C(54.38%), H(3.12%), N(9.76%), Co(10.26%); IR(KBr) ν (cm^{-1}): 1591(s) (HC=N), 1612(m) (C–NO_2), 3402(w) (free OH), 1314(m) (C–O), 415(m) (M–N), 525(s) (M–O), 1468(s) (Ph–C=C), 1529(m) (Ph–C–C), 2930(m) (Ph–C–H) UV-Vis (DMF) [nm (frequency, cm^{-1})(transition)(geometry)]; 556(17,985) [$^4T_1(F) \rightarrow {}^4A_2(F)$] (tetrahedral), 436(22,935) [$^4T_1(F) \rightarrow {}^4T_1(P)$] (tetrahedral), 264(37,878) (ILCT), 221(45,248) (ILCT) magnetic moment, μ_{eff} (BM); 4.51.

CoL_2[3c] (6): light brown, yield 72%, molecular formula: $CoC_{28}H_{24}N_2O_6$, molecular weight: 543.44, m.p.: >250°C, Anal. Calcd C(61.88%), H(4.45%), N(5.15%), Co(10.84%); found: C(61.85%), H(34.38%), N(5.10%), Co(10.82%); IR(KBr) ν (cm^{-1}): 1582(m) (HC=N), 1329(m) (O–CH_3), 3317(m) (free OH), 1319(m) (C–O), 421(m) (M–N), 578(s) (M–O), 1418(m) (Ph–C=C), 1521(m) (Ph–C–C), 2933(w) (Ph–C–H) UV-Vis (DMF) [nm (frequency, cm^{-1})(transition)(geometry)]; 562(17,793)

$[^4T_1(F) \rightarrow {}^4A_2(F)]$ (tetrahedral), 435(22,988) $[^4T_1(F) \rightarrow {}^4T_1(P)]$ (tetrahedral), 265 (37,735) (ILCT), 251(39,840) (ILCT) magnetic moment, μ_{eff} (BM); 4.36.

ZnL_2[1a] (7): greenish yellow, yield 62%, molecular formula: $ZnC_{30}H_{28}N_2O_6$, molecular weight: 577.94, m.p.: 204°C, Anal. Calcd C(62.34%), H(4.88%), N(4.84%), Zn(11.31%); found: C(62.31%), H(4.75%), N(4.78%), Zn(11.28%); ^{1}H-NMR (300 MHz, DMSO-d_6) δ: 3.95(s, 3H, O–CH_3), 6.69–7.01(m, 4H, Ph), 7.35–7.61(m, 3H, Ph), 8.62(s, 1H, N=CH), IR(KBr) ν (cm^{-1}): 1593(s) (HC=N), 1368(w) (O–CH_3), 1312(m) (C–O), 427(m) (M–N), 545(m) (M–O), 1428(s) (Ph–C=C), 1487(m) (Ph–C–C), 2971(s) (Ph–C–H).

ZnL_2[2b] (8): brown, yield 65%, molecular formula: $ZnC_{26}H_{18}N_4O_8$, molecular weight: 579.83, m.p.: 148°C, Anal. Calcd C(53.85%), H(3.13%), N(9.66%), Zn(11.27%); found: C(53.79%), H(3.12%), N(9.58%), Zn(11.24%); ^{1}H-NMR (300 MHz, DMSO-d_6) δ: 3.94(s, 3H, O–CH_3), 6.86–7.02(m, 4H, Ph), 7.14–7.55(m, 3H, Ph), 8.56(s, 1H, N=CH), IR(KBr) ν (cm^{-1}): 1587(m) (HC=N), 1618(w) (C–NO_2), 3381(m) (free OH), 1311(m) (C–O), 427(m) (M–N), 543(s) (M–O), 1482(s) (Ph–C=C), 1528(s) (Ph–C–C), 2938(m) (Ph–C–H).

ZnL_2[3c] (9): light brown, yield 73%, molecular formula: $ZnC_{28}H_{24}N_2O_6$, molecular weight: 549.88, m.p.: >250°C, Anal. Calcd C(61.16%), H(4.40%), N(5.09%), Zn(11.89%); found: C(61.08%), H(4.36%), N(5.03%), Zn(11.87%); ^{1}H-NMR (300 MHz, DMSO-d_6) δ: 3.93(s, 3H, O–CH_3), 6.64–6.99(m, 4H, Ph), 7.16–7.35(m, 3H, Ph), 8.43(s, 1H, N=CH), IR(KBr) ν (cm^{-1}): 1585(m) (HC=N), 1329(m) (O–CH_3), 3381(m) (free OH), 1323(m) (C–O), 432(m) (M–N), 581(s) (M–O), 1419(m) (Ph–C=C), 1527(m) (Ph–C–C), 2938(w) (Ph–C–H).

3. Results and discussion

3.1. *^{1}H-NMR spectra*

^{1}H-NMR spectra of **HL^1**, **HL^2**, and **HL^3** and their zinc complexes were recorded in DMSO-d_6; data along with assignments are provided in section 2. All proton resonances of the aromatic region were assigned. The OH signal in the spectrum of **HL^1** at δ9.86 disappeared in its complex spectrum (**7**), indicating that OH is involved in complexation with Zn(II).

3.2. *Mass spectra*

Mass spectra provide a vital clue for elucidating the structure of compounds. The electronic impact mass spectrum of the **HL^2** showed a molecular ion (M^+) peak at $m/z = 258$ corresponding to $[C_{13}H_{10}N_2O_4]^+$, which confirmed the proposed formula. The different competitive fragmentation pathways of ligand gave peaks at m/z 58, 79, 91, 93, 99, 103, 139, 151, 165, 213, and 257 which are shown in scheme S1 (Supplementary material). The intensities of these peaks give the stability and abundance of the fragments. Complex **8** showed a molecular ion peak at m/z 579 with isotopic peaks at 578, 580, 581, and 582 m/z, suggesting monomeric complex.

The molecular ion peaks shown by other complexes were also in good agreement with the structural formula suggested by elemental analysis, spectral, and magnetic studies.

3.3. *Electronic and magnetic moment studies*

The electronic spectra of ligands and complexes were recorded in DMF from 200 to 1100 nm. The ligands showed absorption of the $\pi \rightarrow \pi^*$ and $n \rightarrow \pi^*$ transitions of C=N chromophore or charge-transfer transition arising from π electron interactions between the metal and ligand, which involves either a metal-to-ligand or ligand-to-metal electron transfer [15, 16].

The n–π^* bands in the complexes show a slight shift due to donation of electrons to the metal and hence, coordination of azomethine, with a reduction of intensity. Strong bands at 229–350 nm are observed in spectra of all Cu(II) complexes. For the Cu(II) complexes there are two spin-allowed transitions, $^2B_{1g} \rightarrow {}^2A_{1g}$ and $^2B_{1g} \rightarrow {}^2E_{1g}$, suggesting SP geometry around Cu(II) [17, 18]. Their magnetic moments support a distorted SP geometry [19].

Two d–d bands were observed in spectra of the cobalt(II) complexes between 581 and 435 nm due to $^4T_1(F) \rightarrow {}^4A_2(F)$ and $^4T_1(F) \rightarrow {}^4T_1(P)$ transitions, in agreement with assignments made earlier for tetrahedral cobalt(II) complexes [20, 21]. Together with the magnetic moment, this gives adequate support to a tetrahedral geometry for the cobalt(II) complexes [22]. High intensity bands at 221–308 nm have been assigned to charge transfer transitions arising from excitation of an electron from the metal to the unfilled molecular orbitals derived from the π^* level of the ligands [23].

Zinc(II) complexes are diamagnetic as expected; its geometry is probably tetrahedral with N, O donor Schiff bases. The electronic spectral data and empirical formula of the zinc(II) complexes are consistent with a tetrahedral geometry [24].

3.4. *Molar conductance measurements*

The chelates were dissolved in DMF and their molar conductivities of 10^{-3} mol L^{-1} solutions at $25 \pm 2^\circ$C were measured. Complexes **1–9** lie in the range 0.74–3.91 Ω^{-1} cm^{-2} mol^{-1} indicating non-electrolytes [25].

3.5. *IR spectra and mode of bonding*

IR spectral data of **HL[1]**, **HL[2]**, and **HL[3]** and their complexes are listed in section 2. The azomethine $\nu_{(C=N)}$ stretch (in free ligand at 1615–1625 cm^{-1}) shifted to lower frequencies in complexes, indicating participation of the azomethine nitrogen in coordination [26]. The stretching frequency at 2845–2852 cm^{-1} for the ligands showed the presence of O–H $\cdots$ N intramolecular hydrogen bonds [27]. This $\nu_{(OH)}$ band (intramolecular H bonding OH) of the free ligands disappeared on complexation, indicating coordination through deprotonated phenolic oxygen. Participation of the OH group was further confirmed by clarifying the effect of chelation on the $\nu_{(C-O)}$ and in-plane bending, $\delta_{(OH)}$ [28]. New bands in spectra of the complexes at 525–581 cm^{-1} were assigned to $\nu_{(M-O)}$ stretch, while bands at 415–432 cm^{-1} to the $\nu_{(M-N)}$ mode. Therefore, the above arguments together with the elemental analyses indicate that the

Table 1. The spin Hamiltonian parameters of Cu(II) complexes in DMSO at 300 K and 77 K.

	g-tensor			Hyperfine constant $\times 10^{-4}$ (cm^{-1})		
Complex	$g_{\parallel}$	$g_{\perp}$	g_{iso}	$A_{\parallel}$	$A_{\perp}$	A_{iso}
1	2.74	2.14	2.34	70	260	196
2	2.76	2.17	2.37	74	262	199
3	2.79	2.15	2.36	79	265	203

ligand is monobasic bidentate in coordination *via* the azomethine N and deprotonated phenolic O [29].

3.6. *EPR spectra*

EPR spectra of the Schiff-base complexes were recorded for powder and solution samples at RT and LNT, and the results are described in tables 1 and 2. The Cu(II) complexes at room temperature exhibit isotropic signals with g values (table 1) characteristic for axial symmetry [30]. The trend, $g_{||} > g_{\perp} > g_e$ (2.0027) showed that the unpaired electron was localized in the $d_{x^2-y^2}$ orbital of Cu(II) [31]. Exchange coupling between two Cu(II) ions can be explained by the Hathaway expression $G = (g_{||} - 2)/(g_{\perp} - 2)$. When $G > 4.0$, interaction between metal centers is negligible in solid complexes (table 2). The observed values indicate that odd electron density was less on **1** than the other two chelates. Hence, delocalization of the metal d-electrons is greater in **1** than the other two copper complexes.

The EPR parameters $g_{||}$, $g_{\perp}$, g_{av}, $A_{||}$, and $A_{\perp}$ and the energies of the d–d transitions were used to evaluate the bonding parameters α^2, β^2, and γ^2 which may be regarded as a measure of covalency of the in-plane σ-bonding, in-plane π-bonding, and out-of-plane π-bonding, respectively. The values of α^2 and β^2 were estimated from the following expression [32]; lower values of α^2 compared to β^2 indicate that the in-plane σ-bonding is more covalent than the in-plane π-bonding.

$$\alpha^2 = -(A_{||}/0.036) + (g_{||} - 2.0023) + (3/7)(g_{\perp} - 2.0023) + 0.04,$$
$$\beta^2 = (g_{||} - 2.0023)E/ - 8\lambda\alpha^2.$$

According to Hathaway [33], $K_{||} \approx K_{\perp} \approx 0.77$ for the pure in-plane σ-bonding and $K_{||} < K_{\perp}$ for the in-plane π-bonding, while for the out-of-plane π-bonding $K_{||} > K_{\perp}$. In the Cu(II) complexes, $K_{||} > K_{\perp}$ indicates more significant out-of-plane π-bonding than the in-plane π-bonding in metal–ligand π-bonding. K is dimensionless, as a measure of the contribution of s electrons to the hyperfine interaction and is generally found to have a value of 0.30. The K values obtained for all the complexes are in agreement with those estimated by Assour [34] and Abragam and Pryce [35].

3.7. *Thermogravimetric studies*

HL[1] and **2** were subjected to TGA (figure S1, Supplementary material). The TGA profiles from 30 to 200°C are probably due to the loss of hydration, which may be

Table 2. The bonding parameters of Cu(II) complexes in DMSO solution.

Complex	α^2	β^2	γ^2	$K_{\|\|}$	$K_{\perp}$	$K \times 10^{-4}$ (cm^{-1})	G
1	1.03	2.15	1.60	2.21	1.65	326	5.36
2	1.07	2.10	1.86	2.25	1.99	340	4.53
3	1.11	2.00	1.50	2.22	1.66	340	5.34

bound to the hydroxyl group of the ligand by hydrogen bonds. Above 220°C, the complexes decomposed gradually rather than with sharp decomposition, which may be due to fragmentation and thermal degradation of the organic moiety. As the temperature increased, the thermal decomposition of **HL[1]** occurred in one step from 225 to 328°C with 30.23% weight loss (calculated: 31.12%).

The thermogram of **2** indicated two stages of decomposition loss of aldehyde and oxidative degradation of the remainder to CuO. The first stage of decomposition started at 230°C with 21.79% (calculated: 22.14%) corresponding to loss of aldehyde. The second stage of decomposition took place at 409–520°C, consistent with oxidative decomposition of the complex, leading to the formation of metal oxide. No further change was observed from 520°C to 800°C. Apart from evaluating the thermal stability of the metal complex, this study also helped to characterize the complex.

3.8. *XRD and morphology study*

The XRD and morphology studies of the synthesized compounds and their discussions are given in "Supplementary material".

3.9. *DNA unwinding properties*

There is continuing interest in DNA endonucleolytic cleavage reactions activated by metal ions. Cleavage of plasmid DNA can be monitored by agarose gel electrophoresis. Irradiation of pBR322 plasmid DNA in the presence of the complexes was studied to determine the efficiency with which it sensitizes DNA cleavage. This can be achieved by monitoring the transition from the naturally occurring covalently closed circular form (Form I) to the open circular relaxed form (Form II). This occurs when one of the strands of the plasmid is nicked and can be determined by gel electrophoresis of the plasmid. Extended irradiation results in nicks on both strands of the plasmid, which eventually results in its opening to the linear form (Form III). When circular plasmid DNA is subjected to gel electrophoresis, relatively fast migration is observed for the SC form (Form I). Form II migrates slowly and Form III migrates between Form II and Form I [36].

Chemical nuclease activity of **1–3** in the presence of 3-MPA (500 μmol L^{-1}) was investigated using plasmid SC pBR 322 DNA (30 μmol L^{-1}, 0.2 μg) in 50 mmol L^{-1} *Tris*-HCl buffer/5 mmol L^{-1} NaCl (pH 7.2) as shown in figure S2 (Supplementary material). The extent of DNA cleavage, observed by agarose gel electrophoresis, gives the order **2** > **3** > **1**. Complex **2** completely cleaved SC-DNA into its nicked circular form in the presence of 500 μmol L^{-1} MPA, while **1** and **3** did not show significant

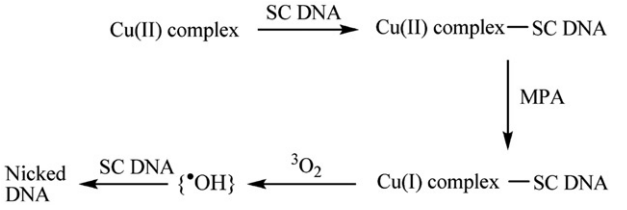

Scheme 2. Mechanistic pathways proposed for chemical nuclease activity by **1**, **2,** and **3**.

chemical nuclease activity under similar conditions. The bulk of $\mathbf{HL^1}$ and $\mathbf{HL^3}$ containing the methoxy substituent could reduce the cleavage activity by lowering DNA binding. Control experiments did not show any cleavage of SC-DNA under similar reaction conditions. The different DNA cleavage of the three complexes may be due to different binding affinity to DNA [37]. The DNA cleavage in the presence of MPA probably proceeds through the hydroxyl radical pathway as proposed by Sigman (scheme 2) [38].

The change in mobility of Form I DNA band with increase in concentration of compounds is due to unwinding of the SC Form I DNA. The increase in intensity of the Form II band with increase in concentration of the compounds is due to partial nicking of Form I DNA to produce Form II DNA [39]. Figure 1 shows gel electrophoresis separation of pBR322 DNA after incubation with **2** and **3** with irradiation at 365 nm. No DNA cleavage was observed for controls in which the complex was absent (lane 1). With increasing concentration of **2** and **3** (figure 1a), the amount of Form I of pBR322 DNA diminished gradually, whereas Form II increased. No obvious DNA SC of Form I to nicked Form II happened at 20 and 40 μmol L^{-1} (for **3**) and 20 μmol L^{-1} (for **2**), indicating that these complexes unwind duplex DNA in a concentration-dependent manner with an activity of DNA cleavage in the order **2** > **3**. At 80 μmol L^{-1}, **2** and **3** promote almost complete conversion of DNA from Form I to Form II. The greater nuclease activity of **2** may be attributed to its redox nature, i.e., the ease of reduction of Cu(II) to Cu(I). At the same concentration of complex, with increasing irradiation time Form II also increased (figure 1b). Similar results have been reported in other cases [40]. Under comparable experimental conditions, **2** exhibited more effective DNA cleavage than **3**.

In order to establish the reactive species responsible for photoactivated cleavage of plasmid DNA, the following experiments were carried out. Photoactivated cleavage of pBR322 in the presence of **2** is shown in figure 2. For **2**, in the presence of different hydroxyl radical scavengers, such as KI, DMSO, and ethanol, different degrees of inhibition in the photo-induced cleavage of the plasmid were observed (figure 2), indicating that hydroxyl radical (OH) is likely the reactive species [41]. Thus photoreduction of **2** with concomitant hydroxide oxidation is the important step in DNA cleavage. DNA incubated with singlet oxygen quenchers histidine, D_2O, and sodium azide were also carried out, and no inhibition was observed, confirming that singlet oxygen radical was not involved in the cleavage.

3.10. *Electrochemical behavior of 1, 4, and 7*

Electrochemical properties of the complexes are described in "Supplementary material".

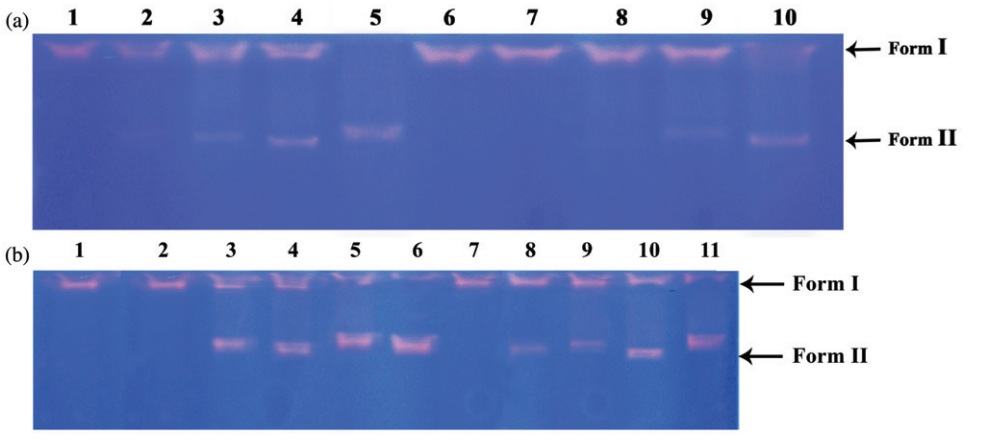

Figure 1. (a) Photoactivated cleavage of pBR322 DNA in the presence of **2** and **3** after 60 min irradiation at 365 nm. Lane 1 and lane 6, DNA alone; lanes 2–5 different concentrations of **2**: (2) 20; (3) 40; (4) 60; and (5) 80 μmol L^{-1}; lanes 7–10, in different concentrations of **3**: (7) 20; (8) 40; (9) 60; and (10) 80 μmol L^{-1}. (b) Photoactivated cleavage of pBR322 DNA in the presence of **2** and **3** (20 mmol L^{-1}) after irradiation at 365 nm for 0, 20, 40, 60, and 80 min (lanes 2–6) for **2** and (lanes 7–11) for **3**, Lane 1, DNA alone.

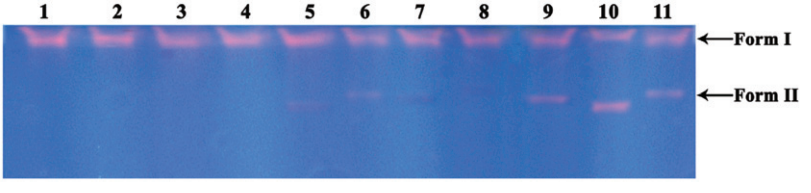

Figure 2. Gel electrophoresis diagram showing the photocleavage of SC pBR 322 DNA by **2** (50 μmol L^{-1}) in the presence of various reagents (30 min) in DMF–*Tris* buffer medium on irradiation with UV light of 365 nm wavelength: Lane 1, DNA control; lane 2, DNA + DMSO (4 μL); lane 3, DNA + ethanol (4 μL); lane 4, DNA + KI (4 μL); lane 5, DNA + **2**; lane 6, DNA + DMSO + **2**; lane 7, DNA + ethanol + **2**; lane 8, DNA + KI + **2**; lane 9, DNA + NaN_3 (5 μL) + **2**; lane 10, DNA + D_2O + **2**; lane 11, DNA + histidine (50 μmol L^{-1}) + **2**.

3.11. *DNA-binding experiments*

Transition metal complexes bind to DNA *via* both covalent and/or non-covalent interactions [42]. In covalent binding, a labile ligand of the complexes is replaced by a nitrogen base of DNA such as guanine N7. Non-covalent DNA interactions include intercalative, electrostatic, and groove (surface) binding of metal complexes outside of the DNA helix. DNA can provide three distinctive binding sites for quinolone metal complexes, groove binding, electrostatic binding to phosphate group, and intercalation [43]. This behavior is of importance to the biological role of quinolone antibiotics in the body [44].

3.11.1. Electronic absorption titration. Electronic spectra are the most common way to investigate interactions of complexes with DNA. For metallo-intercalators, DNA binding causes hypochromism and red shift (bathochromism) due to intercalation

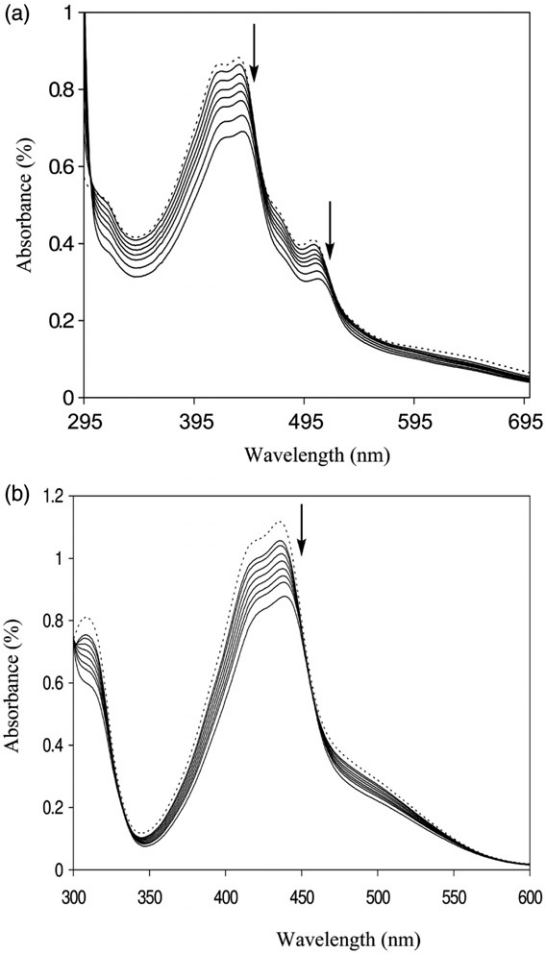

Figure 3. Absorption spectra of (a) **1** and (b) **4** in the presence (——) and absence (- - -) of DNA in *Tris*-HCl buffer upon addition of CT-DNA [complex] = 25 μmol L^{-1}. Arrow shows the absorbance changing upon the increase of DNA concentration.

involving a strong stacking interaction between aromatic chromophore and the base pairs of DNA. Absorption spectra of **1**, **2**, and **3** in the absence and presence of CT-DNA (at [Complex] = 25 μmol L^{-1}) are illustrated in figure 3(a). Upon increasing concentration of DNA, the complexes exhibited pronounced hypochromism, along with a modest bathochromic shift. For **1**, the hypochromism in the MLCT band at 437.5 nm reached as high as 16.47% with a red shift of 6 nm; for **2**, the MLCT band at 441 nm exhibited hypochromism of about 9.78% with a red shift of 6 nm; for **3**, the MLCT band at 438.5 nm exhibited hypochromism of about 15.69% with a red shift of 5.5 nm. Similar hypochromicity was reported for **4** (figure 3b), **5**, and **6** in table 4. These spectral characteristics suggest that the complexes interact with DNA through an intercalation mode, which could subsequently stabilize the DNA duplex [45]. After intercalating the base pairs of DNA, the π^* orbital of the intercalated ligand can couple with the π orbital of the base pairs, thus decreasing the π–π^* transition energy and

Table 3. Electrochemical behavior of Cu(II), Co(II), and Zn(II) complexes in the presence of CT-DNA.

		i_{pc} (A) × 10^{-5}		E_{pc} (V)		$E_{1/2}$ (V)		ΔE_p (V)		
Complex	Redox couple	Free	Bound	Free	Bound	Free	Bound	Free	Bound	K_{oxd}/K_{red}
1	Cu(II)/Cu(I)	1.50	0.89	−0.763	−0.773	0.480	0.478	0.566	0.589	0.67
	Cu(I)/Cu(0)	1.23	0.95	−0.241	−0.255	0.185	0.207	0.852	0.911	1.03
2	Cu(II)/Cu(I)	2.14	2.04	−0.781	−0.799	−0.477	−0.481	0.607	0.636	2.01
	Cu(I)/Cu(0)	1.39	1.18	−0.206	−0.213	−0.009	−0.028	0.394	0.370	0.76
3	Cu(II)/Cu(I)	1.51	1.26	−0.755	−0.784	−0.424	−0.409	0.662	−0.749	0.32
	Cu(I)/Cu(0)	0.72	0.62	−0.088	−0.096	0.318	0.327	0.813	0.847	1.36
4	Co(III)/Co(II)	2.65	2.33	−0.657	−0.676	0.272	0.259	0.360	0.390	0.48
5	Co(II)/Co(I)	3.70	2.92	−1.046	−1.123	−0.804	−0.830	0.484	0.585	0.05
6	Co(III)/Co(II)	2.53	1.81	−0.808	−0.825	−0.562	−0.592	0.491	0.466	1.94
7	Zn(II)/Zn(I)	2.09	1.45	−0.541	−0.567	0.018	0.023	1.046	1.111	2.75
8	Zn(II)/Zn(I)	0.76	0.40	0.124	0.136	0.344	0.363	0.441	0.455	1.59
9	Zn(II)/Zn(I)	1.99	1.64	−0.963	−0.938	−0.748	−0.803	0.43	0.27	2.64

Table 4. Absorption spectroscopic properties of Cu(II) and Co(II) complexes on binding to CT-DNA.

	λ_{max} (nm)[a]				
Complex	Free	Bound	Bathochromism $\Delta\lambda$ (nm)[b]	Hypochromicity (%)[c]	$K_b \times 10^4$ (mol L^{-1})
1	431.5	437.5	6.0	16.47	2.56
2	435	441	6.0	9.78	3.83
3	433	438.5	5.5	15.69	3.58
4	433	437.5	4.5	17.05	2.53
5	434	440	6.0	8.05	3.92
6	432	438.5	6.5	16.44	3.68

[a]In DMF.
[b]Absorption maximum red shift in the presence of CT-DNA in *Tris*-HCl buffer, pH – 7.2.
[c]Absorbance decrease extent at absorption maximum in the presence of CT-DNA in *Tris*-HCl buffer, pH – 7.2.

resulting in the bathochromism [46, 47]. On the other hand, the coupling π orbital is partially filled by electrons, thus decreasing the transition probabilities and concomitantly resulting in hypochromism [48].

The intrinsic binding constant K_b of complexes (table 4) can be obtained from the decay of the absorbance in the MLCT band with increasing concentration of CT-DNA. In general, a planar extension of the intercalative ligand would increase the strength of the interaction of the complexes with DNA [49]. The binding constants indicate that **2** and **5** bind more strongly than **1**, **3**, **4**, and **6**, as expected, since $\mathbf{HL^2}$ possesses greater planar area and extended π system than $\mathbf{HL^1}$ and $\mathbf{HL^3}$, allowing $\mathbf{HL^2}$ to penetrate more deeply into, and stack more strongly with, the base pairs of DNA. The difference could also be attributed to the different steric effect induced by the substituent groups in the ligand at 3 and 4 positions.

3.11.2. Electrochemical studies. CV is a sensitive technique to determine changes in redox behavior of metallic species in the presence of biologically important molecules [50]. The redox behavior of metallic species is sensitive to the coordination

surrounding the metal center; therefore, metal-based interaction can be detected using this technique.

The quasi-reversible redox couple for each complex in 1 : 2 (DMF : buffer solution) has been studied upon addition of CT-DNA; the shifts of the cathodic E_{pc} potentials are given in table 3.

No new redox peaks appeared after addition of CT-DNA to each complex, but the current intensity of all the peaks decreased significantly, suggesting the existence of an interaction between each complex and CT-DNA. The decrease in current intensity and the i_{pa}/i_{pc} values can be explained in terms of an equilibrium mixture of free and DNA-bound complex to the electrode surface [51, 52].

The electrochemical behaviors of the Cu(II) complexes in DMF (table 3) show two redox couples corresponding to Cu(II)/Cu(I) and Cu(I)/Cu(0) in the absence of CT-DNA. For increasing amounts of CT-DNA, the cathodic potential E_{pc} showed a negative shift, $\Delta E_{pc} = -10$ mV [Cu(II)/Cu(I)] and $\Delta E_{pc} = -14$ mV [Cu(I)/Cu(0)] for **1** (figure S3a, Supplementary material), $\Delta E_{pc} = -19$ mV [Cu(II)/Cu(I)] and $\Delta E_{pc} = -7$ mV [Cu(I)/Cu(0)] for **2** (figure S3b, Supplementary material), $\Delta E_{pc} = -29$ mV [Cu(II)/Cu(I)] and $\Delta E_{pc} = -8$ mV [Cu(I)/Cu(0)] for **3** (figure S3c, Supplementary material), on binding to DNA suggesting that both Cu(II) and Cu(I) forms bind to DNA at different rates. These two peaks showed their reduction behavior in **1**, **2**, and **3**. The first one electron reduction occurs at Cu(II) coordinated to the unsaturated nitrogens and the second at Cu(II) coordinated to saturated oxygen. In the anodic region, two peaks correspond to oxidative behavior of Cu(I)/Cu(II) and Cu(0)/Cu(I) (figure S3(a–c), Supplementary material). These shifts of potentials show that **1**, **2**, and **3** bind to DNA by intercalation.

The shift in $E_{1/2}$ with increasing amounts of DNA indicates a difference in the binding of Cu(II) and Cu(I) to DNA. The net shift in $E_{1/2}$ can be used to estimate the ratio of equilibrium constants K_{2+}/K_{+} for binding of Cu(II) and Cu(I), respectively, to DNA. This is consistent with the unequal values of i_{pc}/i_{pa} which is less than one on increasing the concentration of DNA.

CV has been employed to study the interaction of the redox active Co(II) complexes (**4**, **5**, and **6**) with DNA. Summaries of voltammetric results of three complexes are given in table 3. The CV data of **4** and **6** in the absence of DNA featured reduction of +3 to the +2 form at a cathodic peak potential E_{pc} of −0.657 V for **4** and −0.808 V for **6** *versus* Ag/AgCl; the re-oxidation of the +2 form upon scan reversal occurred at 0.113 and −0.317 V, respectively. In the absence of DNA, the separation of the anodic and cathodic peak potentials, $\Delta E_p = 0.360$ V for **4** and 0.491 V for **6**, indicate a quasi-reversible one-electron redox process. The formal potential $E_{1/2}$, taken as the average of E_{pc} and E_{pa}, are 0.272 and −0.562 V, respectively. Complex **4** showed one more oxidation wave with $E_{pa} = 0.089$ V in the absence of DNA which can be assigned to the oxidation of +1 form as shown in figure S3d (Supplementary material). The presence of DNA in the solution at the same concentration of these two complexes caused a considerable decrease in the voltammetric current. In addition, the peak potentials, E_{pc} and E_{pa}, as well as $E_{1/2}$ shift to less negative potential. The drop of the voltammetric currents in the presence of CT-DNA can be attributed to diffusion of the metal complex bound to the large, slowly diffusing DNA.

CV of **5** exhibited one redox couple corresponding to Co(II)/Co(I) at $E_{pc} = -1.046$ V and $E_{pa} = -0.562$ V with $\Delta E_p = 0.484$ V. In the presence of CT-DNA, at the same concentration of complex, the peak potentials ($E_{pc} = -1.123$ V and $E_{pa} = -0.538$ V) were shifted to less negative potential and the redox couple was quasi-reversible with

$\Delta E_p = 0.585$ V. Thus, the apparent $E_{1/2}$ shifted to more negative potentials by 26 mV in the presence of DNA. In the absence of DNA, the CV of **5** did not show a reduction of +3 to +2 in cathodic peak potential. The change in the substituent in the ligands may affect the oxidation potential of the metal ion, indicating that small changes in the electronic and structural coordination environment affect the redox potential of the complexes. The decrease in the peak currents for these complexes upon addition of CT-DNA indicates that DNA-binding affinity increases in the order **5** < **4** < **6**.

The ligand has a significant effect on $E_{1/2}$ for all the complexes; electron-withdrawing groups stabilize cobalt(II) while electron-donating groups favor oxidation to cobalt(III). Electropotentials of Co(II)/Co(III) couple show sensitivity to the nature of ligand.

In the absence of DNA, CVs of **7**, **8**, and **9** show quasi-reversible Zn(II)/Zn(I) oxidation waves with E_{pa}/E_{pc} at −0.541/0.505, 0.124/0.565, and −0.963/−0.533 V, respectively, and quasi-reversible Zn(II)/Zn(I) reductive waves at $E_{1/2} = 0.018$ V (**7**), 0.344 V (**8**), and −0.748 V (**9**). Since all the complexes have similar coordination geometry, the observed trend can be interpreted by the electron-donating effect of the methoxy. For **7** (figure S3e, Supplementary material), the $K_{Zn(II)}/K_{Zn(I)}$ value was calculated to be 2.75, and for **9**, 2.64, suggesting that both **7** and **9** complexes of Zn(I) and Zn(II) interact with DNA almost to the same extent. The complexes **7**, **8**, and **9** interact with DNA through intercalation mode with the binding ability to DNA in the order **7** > **9** > **8**. Upon addition of CT-DNA, the voltammetric currents of **7**, **8**, and **9** decrease from slow diffusion of the complexes bound to the large DNA molecule.

Differential pulse voltammogram (DPV) experiments were also performed to observe the changes in the formal potential as well as the current density during the addition of DNA to solution due to the intercalative interaction of **7**, **8**, and **9**. The reduction process was monitored at a scan rate of $0.1\,Vs^{-1}$ (figure S4a and figure S4b, Supplementary material). DPV also certifies the changes found in CV experiments and hence zinc complexes with 3,4-disubstituted ligands bind to DNA by intercalation, with effective insertion of the $\mathbf{HL^1}$ and $\mathbf{HL^3}$ between the base pairs of the DNA duplex strand.

3.12. *Viscosity measurements*

Viscosity measurements are sensitive to length change of DNA and regarded as the least ambiguous and the most critical tests of binding mode in solution in the absence of crystallographic structural data. Under appropriate conditions, intercalation of drugs like EB causes a significant increase in the viscosity of DNA solution due to the increase in separation of base pairs of intercalation sites increasing DNA length. Molecules binding exclusively in the DNA grooves cause less pronounced or no change in DNA solution viscosity [53]. The effect of **1**–**9** and EB on the viscosity of rod-like DNA is shown in figure 4. Our results reveal a large increase in the relative viscosity of CT-DNA, indicating that interaction involves intercalation, with the compound binding between two adjacent base pairs [54]. The increase in viscosity produced is similar to that caused by EB. For EB, increasing the ratio of EB to DNA increases relative specific viscosities of DNA. On increasing the amounts of **1**–**9**, the relative viscosity of DNA

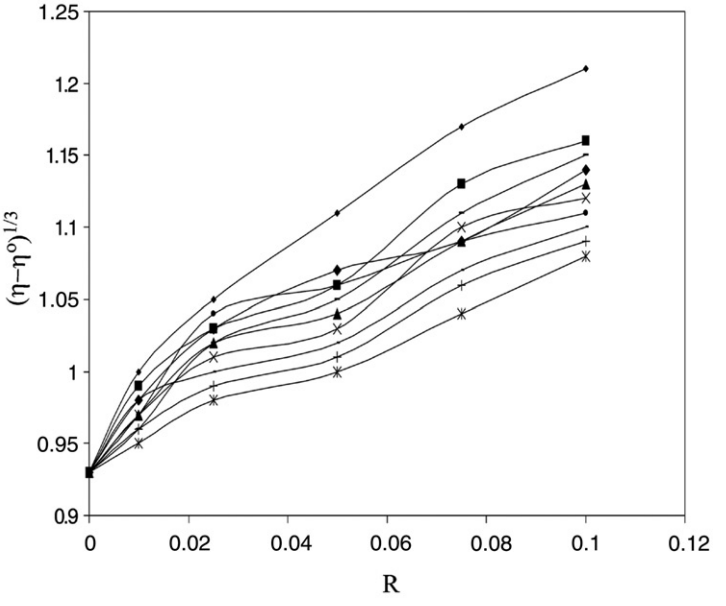

Figure 4. Effect of increasing amounts of EB (♦) and in the presence of increasing concentrations of copper complexes of **1** (_), **2** (+), **3** (•), **4** (×), **5** (*), **6** (−), **7** (■), **8** (▲) and **9** (♦) on the relative viscosity of CT-DNA at 30°C. [DNA] = 1.5 mmol L^{-1}, R = [complex]/[DNA] or [EB]/[DNA].

increased steadily, correlating with DNA-intercalating potential, in the order EB > **7** > **1** > **9** > **8** > **4** > **3** > **6** > **2** > **5**. These complexes bind to DNA through intercalation, consistent with absorption spectra titration, and reflect the tendency of each ligand to intercalate into DNA base pairs.

3.13. *Antimicrobial activity*

Antimicrobial activity of metal complexes generally depends on chelation ability of the ligand, the nature of nitrogen donor ligands, the total charge of the complex, the existence and nature of the metal ion, and the nuclearity of the metal center in the complex [55].

Results shown in table 5 clearly indicate that inhibition is much larger by metal complexes than free ligand. Higher activity of Cu(II) complexes is probably due to effective chelation. This activity is quite comparable to the reference drugs streptomycin/nystatin for bacterial/fungal ($<2.45\,\mu g\,mL^{-1}$) test, respectively. However, the reduced activities in some cases can be attributed to the inability of the complexes to form hydrogen bonds with the cell constituents [56–58].

The results in table 5 show that **1**, **2**, and **3** had the stronger effect against bacteria and fungi than the other complexes used. Complex **8** exhibited higher antibacterial effect against *E. coli* and **5** against *A. niger*, *R. stolonifer*, and *C. albicans* than **1**, **2**, and **3**. Activity is concentration and substituent dependent as the growth of inhibition increases with an increase in concentration of the complexes.

Table 5. MIC (in $\mu g\,mL^{-1}$) of ligands and their metal complexes against Gram-positive and Gram-negative microorganisms.

	Antibacterial activity				Antifungal activity			
Compound	*S. aureus*	*B. subtilis*	*E. coli*	*P. putida*	*A. niger*	*R. stolonifer*	*C. albicans*	*R. bataticola*
1a	32.18	41.27	21.46	42.25	29.48	34.16	36.49	28.17
2b	20.19	36.49	18.76	28.41	29.25	33.24	35.48	28.02
3c	31.28	35.22	20.41	35.41	41.53	38.41	36.40	25.15
1	11.02	13.14	9.87	9.21	10.43	11.87	9.21	9.20
2	7.53	6.58	6.03	8.15	9.14	7.42	9.76	5.24
3	10.24	11.12	11.34	12.14	9.58	9.46	9.14	9.34
4	17.54	19.31	16.75	16.41	21.47	18.73	18.46	17.15
5	9.37	11.34	8.49	8.10	5.28	7.28	8.12	10.51
6	9.63	11.02	8.57	11.98	12.10	7.23	9.54	8.68
7	13.81	15.26	17.54	16.48	15.20	17.31	15.42	17.24
8	9.57	6.84	5.69	10.95	5.67	8.64	11.05	9.18
9	10.64	13.47	14.38	13.64	16.05	12.47	14.39	11.34
Streptomycin	1.98	2.32	1.04	1.16	–	–	–	–
Nystatin	–	–	–	–	1.82	2.45	2.18	1.96

Complexes with electron-withdrawing groups are more active than complexes substituted with electron-donating groups of these complexes.

4. Conclusions

Three Schiff bases and nine complexes have been synthesized and characterized. The experimental data allow assigning SP geometry for Cu(II) complexes and tetrahedral for Co(II) and Zn(II) complexes. The X-ray powder patterns show that the synthesized compounds have orthorhombic systems with formation of amorphous compounds. Spectral titration and viscosity experiments support that the complexes intercalate into DNA base pairs. When irradiated at 365 nm, the complexes are efficient photocleavers of plasmid pBR322 DNA. The hydroxyl radical is likely responsible for cleavage of plasmid pBR322 DNA. Complex **2** promotes cleavage of plasmid pBR322 DNA from the SC Form I to the open circular Form II upon irradiation. In cyclic voltammograms of the complexes, quasi-reversible waves attributed to redox couples, characteristic for each metal complex, have been recorded at potentials expected. Substituents at different positions on the intercalative ligand cause some interesting differences in the properties of the resulting complexes. CV studies show that the complexes bind to CT-DNA by intercalation. A second finding demonstrates the substituent effect of coordinating intrinsically active ligands to bioactive metals in growth inhibition against microorganisms.

Acknowledgments

The authors express their sincere thanks to the College Managing Board, Principal, and Head of the Department of Chemistry, VHNSN College for providing necessary

research facilities. Instrumental facilities provided by Sophisticated Analytical Instrument Facility (SAIF), IIT Bombay, and CDRI, Lucknow are gratefully acknowledged.

References

[1] S. Oshima, N. Hirayama, K. Kubono, H. Kokusen, T. Honjo. *Talanta*, **59**, 867 (2003).
[2] M.H. Youcef, D. Barkat, T. Benabdallah. *J. Saudi. Chem. Soc.*, **10**, 15 (2006).
[3] K. Singh, M.S. Barwa, P. Tyagi. *Eur. J. Med. Chem.*, **42**, 394 (2007).
[4] J. Costamagna, J. Vargas, R. Latorre, A. Alvarado, G. Mena. *Coord. Chem. Rev.*, **119**, 67 (1992).
[5] I. Sakiyan, E. Logoglu, S. Arslan, N. Sari, N. Sakiyan. *Biometals*, **17**, 115 (2004).
[6] C.S. Chow, J.K. Barton. *Methods Enzymol.*, **212**, 219 (1992).
[7] B.D. Wang, Z.Y. Yang, P. Crewdson, D.Q. Wang. *J. Inorg. Biochem.*, **101**, 1492 (2007).
[8] H. Xu, K.C. Zheng, H. Deng, L.J. Lin, Q.L. Zhang, L.N. Ji. *Dalton Trans.*, **3**, 2260 (2003).
[9] H. Xu, K.C. Zheng, Y. Chen, Y.Z. Li, L.J. Lin, H. Li, P.X. Zhang, L.N. Ji. *Dalton Trans.*, **11**, 2260 (2003).
[10] M. Asadi, E. Safaei, B. Ranjbar, L. Hasani. *New J. Chem.*, **28**, 1227 (2004).
[11] T. Gupta, A.K. Patra, S. Dhar, M. Nethaji, A.R. Chakravarty. *J. Chem. Sci.*, **117**, 123 (2005).
[12] R.K. Dubey, U.K. Dubey, C.M. Mishra. *Indian J. Chem.*, **47A**, 1208 (2008).
[13] Y. Zhang, Y. Shen, Y. Li, Y. Wang, Y. Li, X. Tao, H. Xu. *Inorg. Chim. Acta*, **361**, 2279 (2008).
[14] M.V. Angelusiu, S.F. Barbuceanu, C. Draghici, G.L. Almajan. *Eur. J. Med. Chem.*, **45**, 2055 (2010).
[15] E. Tas, M. Aslanoglu, A. Kilic, Z. Kara. *J. Coord. Chem.*, **59**, 861 (2006).
[16] M. Odabasoglu, F. Arslan, H. Olmez, O. Buyukgungor. *Dyes Pigm.*, **75**, 507 (2007).
[17] A. Biswas, M.G.B. Drew, A. Ghosh. *Polyhedron*, **29**, 1029 (2010).
[18] N. Raman, R. Jeyamurugan, A. Sakthivel, L. Mitu. *Spectrochim. Acta, Part A*, 75, 88 (2010).
[19] K. Mohanan, B. Murukan. *Synth. React. Inorg. Met.: Org. Nano-Met. Chem.*, **35**, 837 (2005).
[20] S. Budagumpi, V.K. Revankar. *Spectrochim. Acta, Part A*, **77**, 184 (2010).
[21] E.K. Beloglazkina, A.G. Majouga, I.V. Yudin, N.V. Zyk, A.A. Moiseeva, K.P. Butin. *Russ. Chem. Bull. Int. Edn.*, **54**, 2163 (2005).
[22] M. Cheriyan, K. Mohanan. *Asian J. Chem.*, **19**, 2831 (2007).
[23] N. Dharmaraj, P. Viswanathamurthi, K. Natarajan. *Transition Met. Chem.*, **26**, 105 (2001).
[24] A.A.A. Emara. *Spectrochim. Acta, Part A*, **77**, 117 (2010).
[25] S. Chandra, D. Jain, A.K. Sharma. *Spectrochim. Acta, Part A*, **71**, 1712 (2009).
[26] J.R. Ferrero. *Low-Frequency Vibrations of Inorganic and Coordination Compound*, John Wiley & Sons, New York (1971).
[27] H. Nazır, M. Yıldız, H. Yılmaz, M.N. Tahir, D. Ülkü. *J. Mol. Struct.*, **524**, 241 (2000).
[28] M.M. Omar, G.G. Mohamed. *Spectrochim. Acta, Part A*, **61**, 929 (2005).
[29] U.O. Ozdemir, F. Arslan, F. Hamurcu. *Spectrochim. Acta, Part A*, **75**, 121 (2010).
[30] S.M. Abdallaha, G.G. Mohamed, M.A. Zayedb, M.S. Abou El-Ela. *Spectrochim. Acta, Part A*, **73**, 833 (2009).
[31] K.B. Gudasi, S.A. Patil, R.S. Vadavi, R.V. Shenoy. *Transition Met. Chem.*, **31**, 586 (2006).
[32] D. Kivelson, R. Neiman. *J. Chem. Soc., Dalton Trans.*, **35**, 149 (1961).
[33] B.J. Hathaway. *Structure and Bonding*, Vol. 14, p. 60, Springer-Verlag, Heidelberg (1973).
[34] M. Assour. *J. Chem. Phys.*, **43**, 2477 (1965).
[35] A. Abragam, M.H.L. Pryce. *Proc. R. Soc. London, Ser. A*, **206**, 164 (1951).
[36] X.W. Liu, J. Li, H. Li, K.C. Zheng, H. Chao, L.N. Ji. *J. Inorg. Biochem.*, **100**, 385 (2006).
[37] X.L. Wang, H. Chao, H. Li, X.L. Hong, Y.J. Liu, L.N. Ji. *Transition Met. Chem.*, **30**, 305 (2005).
[38] D.S. Sigman, A. Mazumder, D.M. Perrin. *Chem. Rev.*, **93**, 2295 (1993).
[39] M.A. Chowdhury, F. Huq, A. Abdullah. *J. Inorg. Biochem.*, **99**, 1098 (2005).
[40] Y.J. Liu, H. Chao, L.F. Tan, Y.X. Yuan, W. Wei, L.N. Ji. *J. Inorg. Biochem.*, **99**, 530 (2005).
[41] N. Raman, A. Sakthivel, R. Jeyamurugan. *J. Coord. Chem.*, **63**, 1080 (2010).
[42] Q.L. Zhang, J.G. Liu, H. Chao, G.Q. Xue, L.N. Ji. *J. Inorg. Biochem.*, **83**, 49 (2001).
[43] B.M. Zeglis, V.C. Pierre, J.K. Barton. *Chem. Commun.*, **2007**, 4565 (2007).
[44] G.S. Son, J.A. Yeo, M.S. Kim, S.K. Kim, A. Holmen, B. Akerman, B. Norden. *J. Am. Chem. Soc.*, **120**, 6451 (1998).
[45] E.C. Long, J.K. Barton. *Acc. Chem. Res.*, **23**, 271 (1990).
[46] N. Raman, A. Sakthivel, R. Jeyamurugan. *J. Coord. Chem.*, **62**, 3969 (2009).
[47] N. Raman, R. Jeyamurugan, R. Usha Rani, T. Baskaran, L. Mitu. *J. Coord. Chem.*, **63**, 1629 (2010).
[48] E.K. Efthimiadou, A. Karaliota, G. Psomas. *J. Inorg. Biochem.*, **104**, 455 (2010).

[49] A.M. Pyle, J.K. Barton. In *Progress in Inorganic Chemistry: Bioinorganic Chemistry*, S.J. Lippard (Ed.), Vol. 38, p. 413, Wiley, New York (1990).
[50] S. Srinivasan, J. Annaraj, P.R. Athappan. *J. Inorg. Biochem.*, **99**, 876 (2005).
[51] S. Tabassum, S. Parveen, F. Arjmand. *Acta Biomater.*, **1**, 677 (2005).
[52] N. Raman, A. Sakthivel, K. Rajasekaran. *J. Coord. Chem.*, **62**, 1661 (2009).
[53] S. Satyanarayana, J.C. Dabroniak, J.B. Chaires. *Biochemistry*, **32**, 2573 (1993).
[54] N. Raman, R. Jeyamurugan. *J. Coord. Chem.*, **62**, 2375 (2009).
[55] G. Psomas, A. Tarushi, E.K. Efthimiadou, Y. Sanakis, C.P. Raptopoulou, N. Katsaros. *J. Inorg. Biochem.*, **100**, 1764 (2006).
[56] R.P. John, A. Sreekanth, V. Rajakamman, T.A. Ajith, M.R.P. Kurup. *Polyhedron*, **23**, 2549 (2004).
[57] A.N.M.A. Alaghaz, R.A. Ammar. *Eur. J. Med. Chem.*, **45**, 1314 (2010).
[58] B.G. Tweedy. *Phytopathology*, **55**, 910 (1964).